Origin and tuning of the magnetocaloric effect for the magnetic refrigerant $MnFe(P_{1-x}Ge_x)$

Danmin Liu[1,2], Ming Yue[1] Jiuxing Zhang[1], T. M. McQueen[3], Jeffrey W. Lynn[2]*, Xiaolu Wang[1], Ying Chen[2,4], Jiying Li[2,4], R. J. Cava[3], Xubo Liu[5], Zaven Altounian[5], Qingzhen Huang[2]

[1]Key Laboratory of Advanced Functional Materials Ministry of Education, Beijing University of Technology, 100 Pingleyuan, Chaoyang District, Beijing 100022, China
[2] NIST Center for Neutron Research, National Institute of Standards and Technology, Gaithersburg, MD 20899
[3] Department of Chemistry, Princeton University, Princeton, NJ 08544
[4] Department of Materials Science and Engineering, University of Maryland, College Park, MD 20742
[5] Center for the Physics of Materials and Department of Physics, McGill University, 3600 University street, Montreal, Quebec, H3A 2T8, Canada

Neutron diffraction and magnetization measurements of the magneto refrigerant $Mn_{1+y}Fe_{1-y}P_{1-x}Ge_x$ reveal that the ferromagnetic and paramagnetic phases correspond to two very distinct crystal structures, with the magnetic entropy change as a function of magnetic field or temperature being directly controlled by the phase fraction of this first-order transition. By tuning the physical properties of this system we have achieved a maximum magnetic entropy change exceeding 74 J/Kg K for both increasing and decreasing field, more than twice the value of the previous record.

PACS: 75.30.Sg; 75.30.Kz; 64.70.K-; 61.05.fm

Recently, magnetic refrigeration at ambient temperatures has attracted interest with the discovery of new materials with improved efficiencies and advantages, as potential replacements for the classical vapor compression systems in use today [1-6]. In particular, Pecharsky *et al* [2] reported that $Gd_5(Ge_2Si_2)$ has a giant MCE between 270 and 300 *K*, while Tegus *et al.* [6] found that $MnFe(P_{1-x}As_x)$ with the hexagonal Fe_2P-type structure has a paramagnetic-ferromagnetic phase transition that is strongly first order and exhibits a huge MCE. In addition, the Curie temperature (T_c) and hence optimal operating temperature of this latter material can be varied from 200 to 350 *K* by tuning the P/As ratio without losing the large MCE [6]. However, the high cost of Gd, and the toxicity of As, make it questionable whether either material will be viable commercially on a wide scale. On the other hand, recently the replacement of As by Ge (or Si) has been reported to still provide a very large MCE (up to 38 J/Kg-K for a field change of 5 T [7-15]), circumventing the toxicity issue and thereby demonstrating its potential as a cost effective and environmentally friendly refrigerant [10,12-14]. For the particular material chosen to study here, we find that $Mn_{1.1}Fe_{0.9}P_{0.8}Ge_{0.2}$ is single phase and paramagnetic at higher temperature, single phase and ferromagnetic at lower temperature, and in between the system undergoes a strongly first-order phase transition as a function of temperature or applied magnetic field. Both phases possess the same symmetry space group ($P\bar{6}2m$) but have distinctly different structures; the *a*- and *b*-axes are ~1.3% longer while the *c*-axis is contracted by ~2.6% in the ferromagnetic (FM) phase compared to the paramagnetic (PM) phase. The large MCE then originates from converting one phase to the other. Thus, by using the Maxwell relations method discussed in ref [16] and [17] we obtained the maximum magnetic entropy changes, from which the isothermal magnetization in both magnetic field increasing and decreasing mode, of 74 and 78 J/Kg K, respectively, for a field change of 5 T in a bulk $Mn_{1.1}Fe_{0.9}P_{0.8}Ge_{0.2}$ compound (as shown in Fig. 1), twice the previous value for this system and the highest MCE for any material presently known [13, 14]. The improved properties and overall advantages of this material open the possibility for wide scale magnetic refrigerant applications using this material.

The starting materials for the polycrystalline samples used in this work were submitted to ball milling, which was carried out under argon atmosphere for 1.5 hour in a high energy Pulverisette

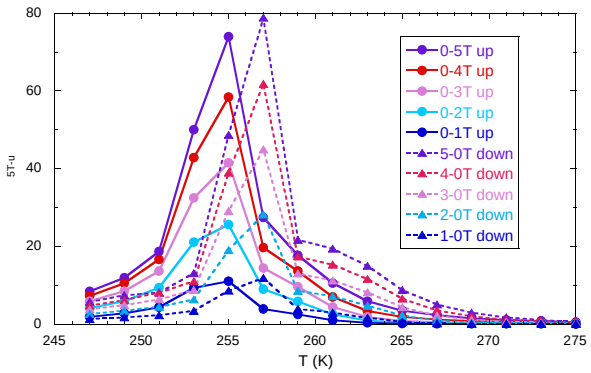

Fig. 1. (color online) Temperature dependence of the magnetic entropy change of the bulk $Mn_{1.1}Fe_{0.9}P_{0.8}Ge_{0.2}$ compound as a function of applied magnetic field up to 5 T.

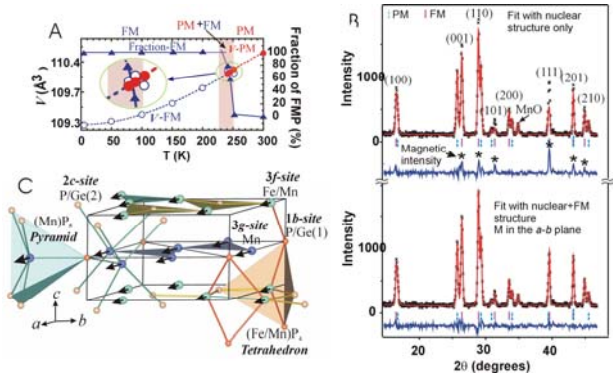

Fig. 2. (color online) (a) Phase fraction and unit cell volume as a function of temperature. (b) Portion of the high resolution neutron diffraction pattern at 245 K. The upper panel shows a fit with only the nuclear structure model, where the difference between the observed and calculated intensities indicates the ferromagnetic peak intensities. An excellent fit was achieved by including a ferromagnetic model with the moments in the *a*-*b* plane (lower panel). The vertical solid and dotted lines show the structural Bragg peak positions for the ferromagnetic phase and paramagnetic phase, respectively. (c) Crystal structure with the magnetic moments (arrows) of the transition metal ions aligned ferromagnetically in the *a*-*b* plane.

4 mill. The milled powders were collected into a graphite mold and consolidated into a Φ20×5 mm^2 wafer sample at 1173 K under 30 MPa by the spark plasma sintering technique. The density of the sample was determined by the Archimedes method to be over 95% of the density of the as-cast ingot. Three 4×4×20mm bars were cut and used for the neutron diffraction experiments. But the solid bars broke into powder after measurements in which magnetic fields up to 7 T were applied together with cooling and warming between 200 *K* and 300 *K*. The results reported in this paper were obtained from the broken powder and are reproducible on cycling temperature or magnetic field. Neutron powder diffraction (NPD) data were collected at the NIST Center for Neutron Research on the high resolution powder neutron diffractometer (BT1) with monochromatic neutrons of wavelength 1.5403 Å produced by a Cu(311) monochromator. Data were collected in the 2θ range of 3º to 168º with a step size of 0.05° for various temperatures from 300 K to 5 K to elucidate the magnetic and crystal structure transitions. Magnetic field measurements were carried out with a vertical field 7 T superconducting magnet. Refinements of the nuclear and magnetic structures in this system were carried out using neutron powder diffraction data and the program GSAS [18]. The sample contains about 1% MnO impurity phase that was taken into account in the refinements.

The refined phase fraction and unit cell volume calculated from neutron diffraction data as functions of temperature for bulk $Mn_{1.1}Fe_{0.9}P_{0.8}Ge_{0.2}$ are shown in Fig. 2(a). The system has a paramagnetic state above ~260 K, a ferromagnetic state below 200 K, with the two phases coexisting in between. No significant change in the unit cell volume was observed during the phase transition. Figure 2(b) shows diffraction data for a temperature of 245 K, where 40% PM-phase equilibrates with 60% FM-phase. Only a portion of the diffraction pattern is shown for clarity. An excellent fit to the data is provided by the crystal structure shown in Fig. 2(c), along with a ferromagnetic structure (*P11m′* magnetic symmetry) having Mn and Fe moments parallel in the *a*-*b* plane. Refined ferromagnetic moments at 245 K are 2.9(1) and 0.9(1) μ_B for the Mn (3*g*) site and Fe/Mn (3*f*) site, respectively, similar to what is seen for other compounds with the Fe_2P-type structure where a larger moment (~3 μ_B) is found at the 3*g* site and a smaller moment (<1 μ_B) at the 3*f* site [10,15]. The moment direction is different from $MnFeP_{1-x}As_x$, which lies in the *a*-*c* plane or along the *c*-axis [15], but we found that fits with a component of the moments parallel to the *c*-axis gave significantly worse agreement with our data. We remark that once the FM-phase is established, no significant changes in the crystal or magnetic structures of the FM-phase were observed on further cooling or applying a higher magnetic field. Therefore magnetic field, or temperature, has no significant effect other than to convert the system between the ferromagnetic and paramagnetic structural phases. The refined Mn/Fe ratio of 1.072(6)/0.928(6) is very close to the nominal ratio of Mn/Fe=1.1/0.9. We find that the 3*g* site is completely occupied by Mn atoms, which is co-planar with

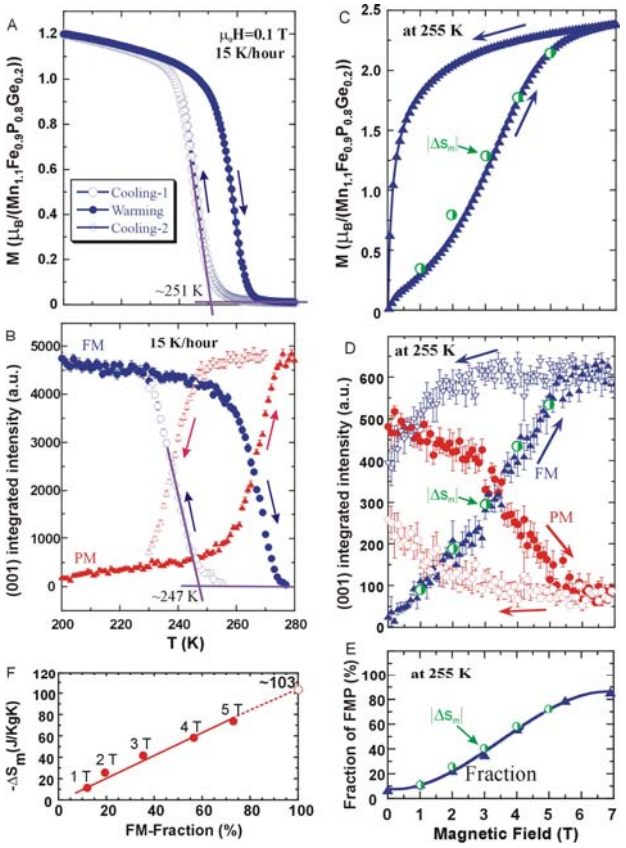

Figure 3. (color online) (a) Temperature dependence of the magnetization in an applied field of 0.1 Tesla and rates of 15 K/hr cooling and warming. The material is not in thermodynamic equilibrium in the transition region due to the strong hysteresis. (b) Integrated intensities of the (001) reflections for the PM- and FM- phases as a function of temperature on cooling and warming. In zero field, the magnetic moments in the FM-phase near the Curie temperature are ~3 and ~1 μ_B for the Mn and Fe/Mn sites, respectively, and increase continuously to ~3.5 and ~1.7 μ_B on cooling to 5 K. (c) Field-dependent magnetization at 255 K. The magnetic entropy change $|\Delta S_m|$ (Fig. 1), normalized to the magnetization [19], is shown for comparison. (d) Field dependence of the integrated intensities of the (001) reflections for the PM-phase and FM-phase at 255 K, showing that the FMP phase fraction tracks the magnetization data. For comparison, data normalized from the magnetic entropy change $|\Delta S_m|$ in the Fig. 1 are also shown. (e) Fraction of the FMP at 255 K as the field increases. The FMP fraction increases smoothly to ~86 %. Data normalized from $|\Delta S_m|$ are shown for comparison. (f) $|\Delta S_m|$ increases linearly with the FM-phase fraction. $|\Delta S_m|$ is projected to be ~103 J/KgK if the transition went to completion for this sample.

P/Ge(1) atoms at the 1*b* site in the *z*=0.5 layer. The 3*f* site has ~93% Fe, with ~7% Mn distributed randomly, and the 3*f* Fe/Mn site is co-planar with the P/Ge(2) atoms at the 2*c* site in the *z*=0 layer. We also find that Ge and P are randomly mixed, although Ge atoms prefer the P/Ge(2) (2*c*) site (~27% Ge occupied) to the P/Ge(1) (1*b*) site (~5% Ge). This differs from $MnFeP_{1-x}As_x$, where Fe and Mn were found to be slightly disordered across both the 3*f* (~4% Mn) and 3*g* (~9% Fe) sites, whereas the As and P were found to have no preferential site selectivity [15]. The structural details can be found in supplementary online material.

The first-order nature of the transition can be readily seen from magnetization data such as shown in Fig. 3(a) as a function of temperature, where the PM-phase↔FM-phase transition clearly has substantial thermal hysteresis. Since the PM-phase and FM-phase are structurally distinct, the two phases can be monitored as a function of temperature or magnetic field by neutron diffraction. For this purpose the (001) reflections of the two phases are well-resolved due to the large difference (~2.6%) in the *c*-axis, and Fig. 3(b) shows the integrated intensities for the PM-phase and FM-phase measured on cooling and warming at a speed of 15 K/hr. The peak positions are almost constant, at ~39.8° and ~41.0° in 2θ for the (001)-PM and –FM-phase, respectively, clearly indicating that this is a first order transition. Detailed measurements of the intensities and angular positions as a function of time were performed on cooling—for example, at 248 K the intensity of the (001)-FM-phase increased and stabilized at ~24% of its maximum after holding for 80 minutes, while at 245 K the intensity increased to ~55% and stabilized after 100 minutes. These time-dependent results allow us to conclude that in thermodynamic equilibrium this material has a single PM-phase above ~260 K and a single FM-phase below ~200 K, and that the two phases coexist in the transition region.

More importantly for the magnetic refrigerant properties, the first-order structural transition can be driven by an external magnetic field as shown in Fig. 3(c) for T = 255 K. At this temperature the diffraction data show that initially 95% of the sample is in the PM-state, which is converted into the FM-state with increasing field as indicated in Fig. 3(d) for the (001) PM-phase (nuclear only) and FM-state (nuclear + magnetic) peaks. The magnetic moments are almost independent of the field, while the unit cell volume of the FM-phase increases slightly and that of the PM-phase decreases slightly above μ_0H=3 T. The FM-phase saturates at ~5.2 T, with significant hysteresis being found on subsequently decreasing the applied field. We remark that error bars where

indicated in this article are statistical in origin and represent one standard deviation.

The similar behavior of these data shows that the variation of the magnetization does in fact coincide with the FM-phase fraction. Refined phase fractions as a function of magnetic field are summarized in Fig. 3(e). The magnetic entropy change $|\Delta S_m|$ for $Mn_{1.1}Fe_{0.9}P_{0.8}Ge_{0.2}$ reported in Fig. 1 can be normalized to the magnetization, (001)-FM intensity, and fraction of FM-phase, and the corresponding values of $|\Delta S_m|$ have been inserted in Fig. 3(c), 2(d), and 2(e), respectively. The excellent agreement and linear relationship between $|\Delta S_m|$ and the FM-phase fraction (Fig. 3(f)) demonstrates that the magnetocaloric effect in the system simply mirrors the FM-phase fraction. Moreover, this investigation indicates that only ~70% of PM-phase was converted into the FM-phase in a field of 5 T. Hence an increase of $|\Delta S_m|$ up to ~100 J/Kg K can be achieved when the phase transformation goes to completion.

The present results directly demonstrate that the transition from the PM-phase to the FM-phase and the associated huge magnetocaloric effect is directly controlled by the first-order structural phase transition between these two phases, and, moreover, that a completed phase conversion will increase the MCE up to ~100 J/Kg K in a field of 5 T in this system. The transition can be driven by temperature or applied magnetic field, and for use as a magnetic refrigerant the field-dependent properties are critical. The substitution of Ge for As removes the toxicity obstacle, which leaves the size of the required field as the primary concern. We have found that an applied field can induce substantial preferred orientation to improve the field properties, and we also expect that the magnetic properties can be optimized with further selective chemical substitutions. The time dependence associated with the transition does tend to reduce the practical MCE available for applications, but the overall improvements and prospects for further advances in performance makes this material the magnetic refrigerant of choice and should enable a wide range of commercial magnetorefrigerant applications.

This work was supported by the National High Technology Research and Development Program of China (2007AA03Z458) and the Key Project of Science & Technology Innovation Engineering, Chinese Ministry of Education (705004). T. M. McQueen gratefully acknowledges support by the National Science Foundation graduate research fellowship program. The work at Princeton was supported by grant NSF-DMR-0703095. Identification of commercial equipment in the text is not intended to imply recommendation or endorsement by the National Institute of Standards and Technology.

References

*Corresponding Author: Jeff.Lynn@nist.gov

1. K. A. Gschneidner, Jr., V. K. Pecharsky, A. O. Tsokol, Rep. Prog. Phys. **68**, 1479 (2005).
2. V. K. Pecharsky, K. A. Gschneidner, Jr., Phys. Rev. Lett. **78**, 4494 (1997).
3. F. X. Hu, B. G. Shen, J. R. Sun, Z. H. Cheng, G. H. Rao, X. X. Zhang, Appl. Phys. Lett. **78**, 3675 (2001).
4. H. Wada, Y. Tanabe, Appl. Phys. Lett. 79, 3302 (2001).
5. T. Mazet, H. Ihou-Mouko, B. Malaman, Appl. Phys. Lett. **89**, 022503 (2006).
6. O. Tegus, E. Brück, K. H. J. Buschow, F. R. de Boer, Nature **415,** 150 (2002).
7. O. Tegus, B. Fuquan, W. Dagula, L. Zhang, E. Brück, P. Z. Si, F. R. de Boer, K. H. J. Buschow, J. Alloys Compd. **396**, 6 (2005).
8. X. W. Li, O. Tegus, L. Zhang, W. Dagula,. E. Brück, K. H. J. Buschow, F. R. de Boer, IEEE Trans. Magn. **39,** 3148–3150 (2003).
9. E. Brück, O. Tegus, L. Zhang, X. W. Li, F. R. de Boer, K. H. J. Buschow, J. Alloys Compd. **383**, 32 (2004).
10. D. T. Cam Thanh, E. Brück, O. Tegus, J. C. P. Klaasse, T. J. Gortenmulder, K. H. J. Buschow, J. Appl. Phys. **99**, 08Q107 (2006).
11. W. Dagula, O. Tegus, X. W. Li, L. Song, E. Brück, D. T. Cam Thanh, F. R. de Boer, K. H. J. Buschow, J. Appl. Phys. **99**, 08Q105 (2006).
12. W. Dagula, O. Tegus, B. Fuquan, L. Zhang, P. Z. Si, M. Zhang, W. S. Zhang, E. Brück, F. R. de Boer, K. H. J. Buschow, IEEE Trans. Magn. **41**, 2778–2780 (2005).
13. A. Yan, K. H. Müller, L. Schultz, O. Gutfleischa, J. Appl. Phys. **99**, 08K903 (2006).
14. Z. Q. Ou, G. Wang, S. Lin, O. Tegus, E. Brück, K. H. J. Buschow, J. Phys. Condens. Matter **18**, 11577 (2006).
15. M. Bacmann, J. L. Soubeyroux, R. Barrett, D. Fruchart, R. Zach, S. Niziol, R. Fruchart, J. Magn. Magn. Mater. **134**, 59-67 (1994).
16. V. K. Pecharsky, K. A. Gschneidner, Jr., J. Appl. Phys. **86**, 565-575 (1999)
17. H. W. Zhang, J. Shen, Q. Y. Dong, T. Y. Zhao, Y. X. Li, J. R. Sun, and B. G. Shen, J. Magn. Magn. Mater., **320**, 1879-1883 (2008)
18. A. C. Larson, R. B. Von Dreele, Los Alamos National Laboratory Report No. LAUR086-748 (1990).(original ref 16)
19. Normalization: $I(H)=[I(5T)/-\Delta S_m(5T)_{max}]\times[-\Delta S_m(H)]$ and $F(H)=[F(5T)/-\Delta S_m(5T)_{max}]\times[-\Delta S_m(H)]$, where $-\Delta S_m(H)$ is the magnetic-entropy at maximum for different H reported in the Fig. 3, and $-\Delta S_m(5T)$ is the $-\Delta S_m(H)$ at H=5 T; I(H) the integrated intensity for different H shown in Fig. 3(d), and I(5T) is the I(H) at H=5 T, and similarly

F(H) is the refined FM-phase fraction for different H shows in Fig. 3(e), and F(5T) is the FI(H) at H=5 T.

Supplementary online material.

Table 1. Structural parameters of $Mn_{1.1}Fe_{0.9}P_{0.8}Ge_{0.2}$ at select temperatures and magnetic fields. Space group $P\bar{6}2m$. Atomic positions: Mn: 3*g*(*x*, 0, 1/2); $Fe_{0.928(6)}/Mn_{0.072(6)}$: 3*f*(*x*, 0, 0); $P_{0.947(8)}/Ge_{0.053(8)}$(1): 1*b*(0, 0, 1/2); $P_{0.726(4)}/Ge_{0.274(4)}$(2): 2*c*(1/3, 2/3, 0). Moments for Mn and Fe were set parallel to the *a* direction (equivalent to the *a*-*b* plane for a powder) in the refinements.

Atom	Parameters	295 K/0 T	245.4 K/0 T		200 K/0 T	255 K/3 T		255 K/6.9 T	
		PM-phase	PM-phase	FM-phase	FM-phase	PM-phase	FM-phase	PM-phase	FM-phase
		100%	40.3(1)%	59.7(1)%	100%	64.7(1)%	35.3(1)%	14(1)%	86(1)%
	a (Å)	6.06137(7)	6.0679(2)	6.1477(2)	6.1605(1)	6.0710(2)	6.1491(2)	6.0643(8)	6.1508(1)
	c (Å)	3.46023(5)	3.4462(3)	3.3583(2)	3.33822(9)	3.4527(1)	3.3658(2)	3.4558(7)	3.3640(1)
	V (Å^3)	110.098(3)	109.890(6)	109.918(6)	109.304(3)	110.207(6)	110.215(8)	110.06(3)	110.219(5)
Mn	*x*	0.5916(3)	0.5946(10)	0.5974(8)	0.5949(1)	0.5923(8)	0.596(1)	0.591(4)	0.5966(8)
	B(Å^2)	0.77(2)	0.62(3)	0.62(3)	0.56(2)	1.09(3)	1.09(3)	1.01(3)	1.01(3)
	M (μ_B)			2.9(1)	3.0(1)		4.3(1)		4.41(9)
Fe/Mn	*x*	0.2527(1)	0.2535(4)	0.2546(3)	0.2558(2)	0.2534(4)	0.2547(6)	0.253(2)	0.2544(3)
	B(Å^2)	0.77(2)	0.62(3)	0.62(3)	0.56(2)	1.09(3)	1.09(3)	1.01(3)	1.01(3)
	M (μ_B)			0.9(1)	1.3(1)		0.1(1)		0.59(8)
P/Ge(1)	*B*(Å^2)	0.55(4)	0.54(4)	0.54(4)	0.57(4)	0.90(4)	0.9(4)	0.82(5)	0.82(5)
P/Ge(2)	*B*(Å^2)	0.55(4)	0.54(4)	0.54(4)	0.57(4)	0.90(4)	0.9(4)	0.82(5)	0.82(5)
	Rp (%)	5.25	6.98		7.99	8.10		8.29	
	wRp (%)	6.65	9.19		10.04	10.18		10.52	
	χ^2	1.276	1.700		1.506	1.091		1.164	
Selected interatomic distances (Å) and angles (degree)									
Mn-Mn		3.180(1)	3.193(3)	3.244(3)	3.247(1)	3.187(3)	3.239(5)	3.18(1)	3.242(3)
Fe/Mn-Fe/Mn		2.653(2)	2.664(4)	2.711(3)	2.720(2)	2.664(4)	2.712(6)	2.65(2)	2.709(3)
Mn- Fe/Mn 2.686(2)		2.693(5)	2.694(4)	2.684(3)	2.686(4)	2.688(8)	2.68(2)	2.694(4)	
Mn- Fe/Mn		2.771(1)	2.757(4)	2.743(3)	2.745(2)	2.769(3)	2.752(6)	2.77(1)	2.748(3)
(Fe/Mn)P_4 tetrahedron									
Fe/Mn-P/Ge(2)	×2	2.3109(6)	2.310(2)	2.329(1)	2.3328(3)	2.312(1)	2.3302)	2.307(6)	2.297(1)
Fe/Mn-P/Ge(1)	×2	2.3039(6)	2.303(2)	2.296(1)	2.2918(2)	2.305(1)	2.299(2)	2.307(6)	2.332(1)
MnP_5 pyramid									
Mn-P/Ge(1)		2.476(2)	2.460(4)	2.475(5)	2.488(3)	2.475(5)	2.486(9)	2.520(5)	2.481(5)
Mn-P/Ge(2)	×4	2.5225(5)	2.523(1)	2.515(1)	2.5098(8)	2.523(1)	2.516(2)	2.520(5)	2.517(1)